



Review

Functional materials with high-efficiency energy storage and conversion for batteries and fuel cells

Bo Peng^{a,b}, Jun Chen^{a,b,*}^a Institute of New Energy Material Chemistry, Nankai University, 94 Weijin Road, Tianjin 300071, People's Republic of China^b Engineering Research Center of Energy Storage and Conversion (Ministry of Education), Chemistry College, Nankai University, 94 Weijin Road, Tianjin 300071, People's Republic of China

Contents

1. Introduction	2806
2. Li-ion battery	2806
2.1. Profile of Li/Li ⁺ system, rechargeable Li-ion battery	2806
2.2. Cathode	2807
2.3. Anode	2808
2.4. Electrolyte	2808
3. Aqueous and non-aqueous atomic/ionic magnesium system, Mg ↔ Mg ²⁺	2809
3.1. Primary Mg battery	2809
3.2. Secondary Mg battery	2809
4. Aqueous molecular/atomic hydrogen and proton system, H ₂ (H) ↔ H ⁺	2809
4.1. Profile of H ₂ (H)/H ⁺ system, hydrogen fuel cells	2809
4.2. Proton exchange membranes	2810
4.3. Electrode/catalyst	2811
4.4. Hydrogen production and storage	2811
5. Conclusions and outlook	2812
Acknowledgements	2812
References	2812

ARTICLE INFO

Article history:

Received 24 January 2009

Accepted 19 April 2009

Available online 24 April 2009

Keywords:

Functional materials

Batteries

Fuel cells

Energy storage and conversion

High efficiency

ABSTRACT

Electrochemical energy storage and conversion with high efficiency and cleanliness is unquestionably one challenge for the sustainable development of the society of human beings. The functional materials can be applied in the systems of electrochemical energy storage and conversion such as in the fields of batteries and fuel cells. For the aspect of energy storage, high efficiency is closely connected with lightweight and high energy density materials, such as hydrogen, lithium, and magnesium. While for energy conversion, two major problems exist namely the diffusion/migration of ions and the transportation of electrons. The properties of the corresponding materials directly affect the solution of these challenges. Thus, in this review we concentrate on the crystal structures and the properties of functional materials applied in electrochemical energy storage and conversion systems with selected primary and secondary batteries and hydrogen fuel cells. In particular, the design, synthesis, structure and property of the materials, containing (1) cathode, anode and electrolyte for non-aqueous Li/Li⁺; (2) various Mg, Mg_xMo₆S₈ (0 < x < 2) Chevrel phase cathode and electrolyte solutions for primary and secondary Mg batteries; (3) proton exchange membranes, electrode catalysts, hydrogen production and storage for aqueous H₂(H)/H⁺ fuel cells. The advantages and disadvantages involved in the batteries and fuel cells using functional materials are also discussed.

© 2009 Elsevier B.V. All rights reserved.

* Corresponding author at: Institute of New Energy Material Chemistry, Nankai University, 94 Weijin Road, Tianjin 300071, People's Republic of China.

Tel.: +86 22 23506808; fax: +86 22 23506808.

E-mail address: chenabc@nankai.edu.cn (J. Chen).

1. Introduction

Energy storage and conversion with high efficiency and cleanliness have a great effect on the sustainable development of world economics and ecology. To replace the traditional fossil fuels, electrochemical energy storage and conversion systems, which include representative primary zinc-manganese dioxide (Zn-Mn) and metal-air (Mg/Al/Zn-air) batteries, secondary/rechargeable nickel-metal hydride (Ni-MH), lithium-ion (Li-ion) and magnesium-ion (Mg-ion) batteries, and fuel cells, offer promising alternatives [1,2]. These batteries and fuel cells cover a scope of applications independent from utility power ranging from portable consumer electronic devices to electric vehicles. Remarkably, most of these systems are based on the lightweight elements in the top rows of the periodic table (Fig. 1) [3]. Of all materials, the highest capacity is 26,590 mAh/g from H to H⁺ in the electrode process of hydrogen fuel cells (calculated by Faraday equation, $Q = nF/M$, where n is the number of electrons, F is the Faraday constant, and M is the equivalent molecular weight). As the lightest metal (equivalent weight 6.94 g/mol and specific gravity 0.53 g/cm³), lithium is a good energy carrier, and is mainly used in rechargeable Li-ion batteries and can deliver a theoretical capacity up to 3860 mAh/g [4]. Similarly, magnesium is another alternative lightweight element. With the benefits of low cost, low toxicity and high safety, magnesium has attracted much research interest in the applications for primary Mg-air and secondary Mg-ion batteries [5]. Obviously, because of the high ratio of valence electrons to atomic nucleus, the lightweight elements in the top rows of the periodic table exhibit higher energy density than other elements. Furthermore, the transportation of their ions with small radius (Li⁺, Mg²⁺ and H⁺ with Pauling ionic radius of 0.60, 0.65 and 8.7×10^{-6} Å, respectively) is easier than that of other larger ions when crossing the electrode and the electrolyte. These features render the lightweight elements effective for batteries and fuel cells.

However, although there has been significant development, there are still many disadvantages that thwart the wide application of batteries and fuel cells. With respect to rechargeable Li or Mg batteries, the slow electrode-process kinetics with high polarization and low rate of ion diffusion/migration and electron conductivity are still the major reasons for the current, related, low energy density, limited capacity and short service life. The cost issue is paramount for the current fuel cells, promoting the search for alternative proton exchange membranes and electrode catalysts. In fact, most of the practical batteries deliver specific energy and capacity far below the theoretical value even under optimum

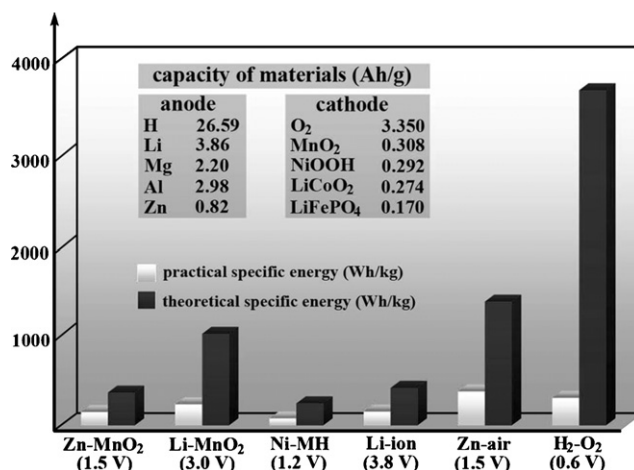


Fig. 2. Theoretical and practical specific energy of Zn-Mn, Li-Mn, Ni-MH, Li-ion and Zn-air batteries plus H₂-O₂ fuel cell with their nominal voltages. The inset table lists the theoretical capacity of the typical electrode materials involved. Data are taken from Ref. [1].

operation conditions (Fig. 2). Since the performance of the batteries and fuel cells depends intimately on the properties of the functional materials included [2,6,7], we here briefly review the recent developments of functional materials that are mainly used in non-aqueous atomic/ionic lithium, aqueous and non-aqueous atomic/ionic magnesium, and aqueous molecular/atomic hydrogen and proton batteries. The aim is to address the demands of finding new functional materials with higher and faster Li/Li⁺, Mg/Mg²⁺, and H/H⁺ storage and conversion.

2. Li-ion battery

2.1. Profile of Li/Li⁺ system, rechargeable Li-ion battery

Different from secondary lead acid and Ni-Cd batteries, Li-ion batteries exhibit the merit of long cycle life, high electrochemical capacity, high energy density and no memory effect [8]. A typical rechargeable Li-ion battery contains a positive electrode (cathode), a negative electrode (anode) and an electrolyte-filled separator with permselectivity for the Li ion (Fig. 3). Commercially, the anode is composed of a carbon material (graphite) and the cathode is constructed by the lithium metal oxide (LiCoO₂, LiMn₂O₄, LiFePO₄, etc.) with a much more positive redox potential, and a Li-ion conducting

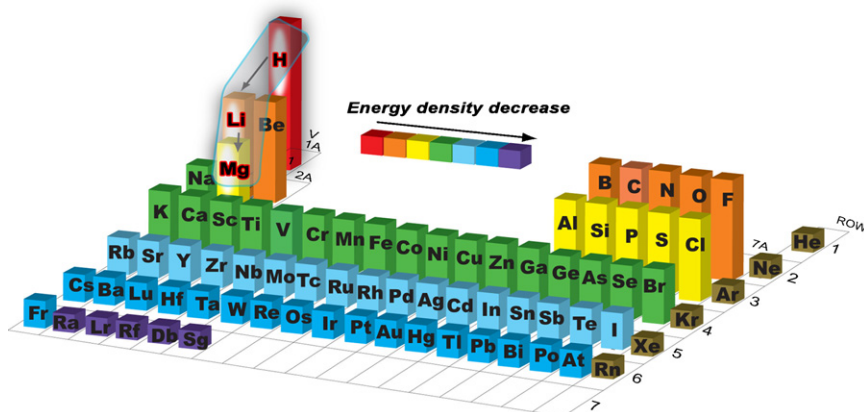


Fig. 1. Schematic diagram showing energy densities (ρ) and how they correlate with the elements in the periodic table. In general, more electronegativity (χ) and less atomic weight (M) will lead to higher energy density for an element in the energy storage and conversion systems. Thus, we have qualitatively estimated the relative energy densities by the equation of $\rho = \chi/M$ for all the elements within the periodic table. Of all materials, the highest capacity is 26,590 mAh/g from H to H⁺. The data of atomic weight and electronegativity for each element are taken from Ref. [3].

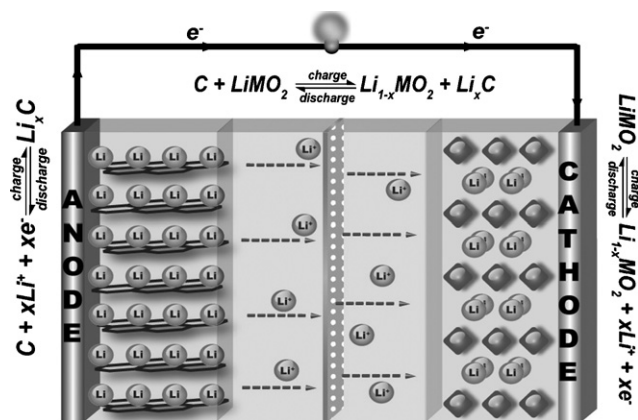


Fig. 3. Profile of a typical rechargeable Li-ion battery and the chemical reactions involved.

electrolyte (LiPF_6 in ethylene carbonate–diethylcarbonate) is filled between the cathode and anode as a separator. The workflow of a rechargeable Li-ion battery can be described as follows. When the Li-ion battery is charged, Li ions are de-intercalated from the cathode, pass across the electrolyte, and finally intercalated between the graphite layers in the anode to form Li_xC alloys. Discharging reverses the process and the whole cycling process activates the electrochemical energy conversion and storage in the batteries.

2.2. Cathode

Commercially, LiCoO_2 , LiNiO_2 , and LiMn_2O_4 intercalation materials and their solid solutions have been used as cathode materials for rechargeable Li-ion batteries [9]. These oxides generally possess layered or tunneled structures for reversible intercalation/de-intercalation of Li ion and high stability to air and moisture, and commonly exhibit a potential region higher than 3 V with flat plateau to host lithium. For example, commercial LiCoO_2 exhibits a high voltage approaching 4 V vs. Li and offers a high specific energy of 1017 Wh/kg^{-1} . The crystal structure of LiCoO_2 (Fig. 4a) is composed of Li-ion layers and CoO_6 layers [10]. The unit structure of the latter is an octahedron in which one Co atom is coordinated by six O atoms. Due to the layered structure, Li ions can intercalate/de-intercalate reversibly [11]. The major problem of the cathode materials of Li-ion battery is that side-reactions with the electrolyte that will lead to the formation of the solid–electrolyte interface (SEI) with the decreasing of the charge storage and the increasing of the safety problem. To overcome this drawback, LiFePO_4 (Fig. 4b) has attracted much attention due to its low toxicity, low cost, high thermal and chemical/electrochemical stability [12]. The crystal

structure of LiFePO_4 is made up of three components: Li ion, FeO_6 irregular octahedron and PO_4 tetrahedron [13]. The six-coordinate Fe–O octahedron shares O atoms with a four-coordinate P–O tetrahedron to form a tunneled structure, and Li atoms lie inside the channels. By *ab initio* calculation, Morgan et al. have found that the intrinsic Li diffusivity along one-dimensional (1D) channels in the [0 1 0] direction of the olivine Li_xMPO_4 ($\text{M} = \text{Mn, Fe, Co, and Ni}$) structure is very high [14]. For example, under reasonable assumptions, such as only nearest-neighbor hops among equivalent sites and no two Li can occupy the same site, the diffusion constant of LiFePO_4 was estimated to be $10^{-8} \text{ cm}^2/\text{s}$ along the [0 1 0] direction (vs. $10^{-13} \text{ cm}^2/\text{s}$ for commercial LiCoO_2). However, the traditional micrometer-sized LiFePO_4 powders suffer from slow diffusion of Li ions. Thus, there must be other factors influencing the performance of LiFePO_4 . One of the factors is considered to the electrical conductivity. Park et al. reported conducting polymer/iron-redox-couple composite cathodes for rechargeable Li-ion batteries, in which a $3d^n/3d^{n+1}$ redox pair (generally first-row transition element) is coupled to the polymer cathode backbone (usually polypyrrole, or PPy, 2.5–4.1 V vs. Li^+/Li) with the hope to broaden the charge–discharge curves over the capacity range [15]. The PPy/ LiFePO_4 (olivine, 3.4 V vs. Li^+/Li) showed the increased specific capacity and rate capacity, and the decreased overpotential at high discharge. By using the cryogenic decomposition of RuO_4 at low temperature, Hu et al. introduced RuO_2 (ca. 5 nm) as an electronic conducting nanoscale interconnect for carbon-containing porous LiFePO_4 (pore size ca. 50 nm) to improve electrode performance [16]. Nanosized RuO_2 keeps good contact with the original C- LiFePO_4 and the heterogeneous C- $\text{LiFePO}_4/\text{RuO}_2$ electrode generated, showing improved kinetics and rate capacity at high rates (up to 30 C). In addition to electrical conductivity, Li ion transport along the surface may also be important, since LiFePO_4 exchanges Li ion with the electrolyte on all surface facets, but only [0 1 0] direction offers the 1D channel into the bulk. Therefore, electrode performance of LiFePO_4 should closely depend on the diffusion across the surface towards the (0 1 0) facet. In a very recent example, Kang and Ceder reported coating lithium phosphate on the surface of nanoscale LiFePO_4 could lead to extremely high-rate (200–400 C) performance and ultrafast (10–20 s) charging/discharging [17]. In fact, the coated LiFePO_4 was an off-stoichiometric $\text{LiFe}_{1-2y}\text{P}_{1-y}\text{O}_{4-\delta}$ ($y=0.05$), which is a stable Li-ion conductor and can be further doped with transition metals to enhance the electrical conductivity.

There is also intensive investigation on the use of metal oxides as cathode materials for rechargeable Li-ion battery, of which vanadium pentoxide and manganese oxide are typical intercalation compounds. For the former case, there have been many reports over the past years about the different morphologies of V_2O_5 such as 1D [18], 2D [19], and 3D ordered macroporous elec-

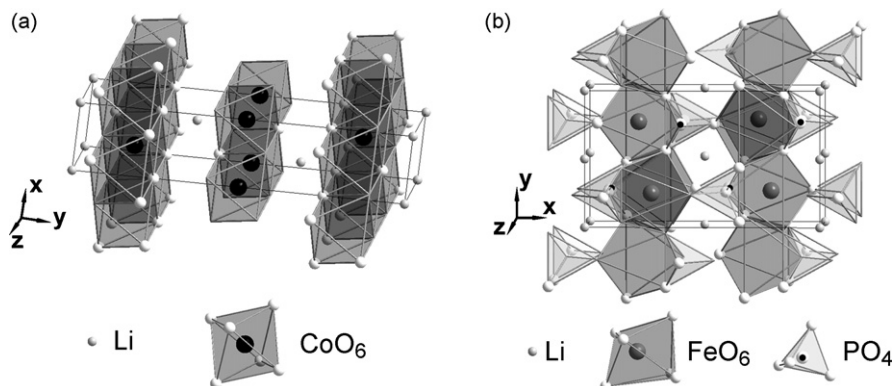


Fig. 4. Crystal structures of LiCoO_2 and LiFePO_4 . (a) LiCoO_2 : $a=b=2.9557(4) \text{ \AA}$, $c=14.532(3) \text{ \AA}$; $\alpha=\beta=90^\circ$ and $\gamma=120^\circ$; space group, $R\bar{3}m$; data are taken from Ref. [10]. (b) LiFePO_4 : $a=10.3290(3) \text{ \AA}$, $b=6.0065(2) \text{ \AA}$, and $c=4.6908(2) \text{ \AA}$; space group, $Pnma$; data are taken from Ref. [13].

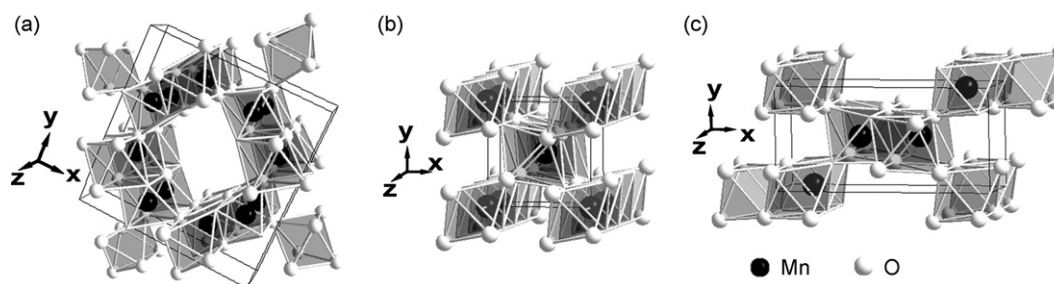


Fig. 5. Crystal structures of α -, β -, and γ - MnO_2 . (a) α - MnO_2 : $a = b = 9.815(1)$ Å and $c = 2.847(1)$ Å; space group, $I4/m$; data are taken from Ref. [21]. (b) β - MnO_2 : $a = b = 4.4041(1)$ Å and $c = 2.8765(1)$ Å; space group, $P42/mnm$; data are taken from Ref. [22]. (c) γ - MnO_2 : $a = 9.3229(11)$ Å, $b = 4.4533(7)$ Å, and $c = 2.8482(3)$ Å; space group, $Pnam$; data are taken from Ref. [23].

trode with nanosized features [20]. Accordingly, short diffusion distance, reduced internal resistance, and high surface area of the nanomaterials have improved the electrochemical kinetics and ionic/electronic diffusion. For manganese oxides, nanocrystals of α -, β -, and γ - MnO_2 , where manganese lies in the octahedral site of oxygen (Fig. 5) [21–23], have been reported as cathode materials [24–27]. Nanostructures of β - MnO_2 with the rutile structure show low capacity and poor cycling stability, while nanostructures of α - MnO_2 (hollandite-type) and γ - MnO_2 demonstrate favorable electrochemical performance. This change is because the bulk or nanostructured β - MnO_2 rapidly converts to LiMn_2O_4 spinel upon Li intercalation, resulting in unfavorable electrochemical performance. However, mesoporous β - MnO_2 displays a remarkably high Li intercalation capacity of 284 mA h/g, corresponding to a composition of $\text{Li}_{0.92}\text{MnO}_2$ [28]. There is also an effort focusing on the intercalation of polymer (poly(diallyldimethylammonium chloride), PDDA) into layered manganese oxides, since the novel structure of the intercalated layered manganese oxides provides the unique function of adjusting the interlayer distance [29].

2.3. Anode

Metals and semiconductors, such as Al, Si, Sn and Bi that can store lithium, are competitive new candidates for anodes in rechargeable Li-ion batteries. During the electrochemical processes, these materials react with Li to form alloys, which can provide much larger specific capacity than that of traditional carbon materials. Typically, silicon can react with Li to form Li–Si alloys, whose fully lithiated composition is $\text{Li}_{4.4}\text{Si}$, and has the highest known theoretical charge capacity of 4200 mA h/g (vs. 372 mA h/g for graphite) [30]. However, the volume of Si anode changes by 400% upon Li intercalation/de-intercalation. Furthermore, the mechanical strain generated leads to remarkable pulverization and capacity fading in just a few electrochemical cycles, which limits its application. Wilson and Dahn reported that carbon-containing nanodispersed Si exhibited a reversible specific capacity of 500 mA h/g [31]. Recently, our group has prepared nest-like (hollow) Si nanospheres by a solvothermal method. The hollow Si nanospheres (90–110 nm in diameter) are composed of ultra-thin Si nanowires with diameters of 5–10 nm and show enhanced high-rate capacity and cycling performance with a nearly 100% coulombic efficiency [32]. By using a vapor–liquid–solid (VLS) method, Chan et al. further assembled a Si nanowire anode Li-ion battery, allowing better accommodation for large strain without pulverization [33].

Although the control of size as well as shape can cycle lithium better than the equivalent bulk materials, they are unable to sustain hundreds of cycles. One alternative is to utilize active–inactive composite materials. The active component reacts with Li whereas the inactive component offers sufficient free space to buffer the volume variations and prevents the nanoparticles aggregation when

cycling. Liu and coauthors have reported that Si–C nanocomposites have shown a high specific capacity of 3257 mA h/g for more than 20 cycles [34]. Scrosati's group has recently presented a new type electrode formed by Ni_3Sn_4 intermetallic nanoalloy, which is electrodeposited on a nanoarchitected Cu substrate [35]. The specific capacity of the assembled Li-ion battery maintains a high specific capacity of about 500 mA h/g over 200 charge/discharge cycles without any significant decay.

To extend the concept, hierarchical 3D mix conducting networks have also been introduced to enhance the migration of Li ion and electron. Early investigations on the anode materials of Li-ion batteries involve transition-metal oxides such as Fe_2O_3 , Co_3O_4 , TiO_2 and NiO, whose full electrochemical reduction migrate two or more electrons per 3d-metal by a “conversion reaction” over hundreds of cycles [36–39]. The composite materials during the discharge process consist of metallic particles (2–8 nm) dispersed in amorphous Li_2O matrix. The so-called “conversion reaction” can be extended to sulfides, nitrides or fluorides. Fluorides generally yield higher potentials than other compounds due to the weaker M–F bonding than M–X (X = O, S, and N), which leads to adjustable voltage and capacity of the cell with the selection of different 3d-metal and its corresponding oxidation state [40].

Recently, Aymard and coworkers demonstrated that metal hydrides are promising as anodes in Li-ion batteries [41] with the advantage of having high capacities in a safe potential window of 0.1–0.5 V vs. Li^+/Li and exhibiting the lowest polarization compared to the reported M_yX_z (M = metal; X = P, N, S, O, and F) electrode. This study bridges the Li-ion battery and hydrogen storage technologies and is believed to promote the realization of electrochemical energy storage and conversion system for mobile applications in the future.

2.4. Electrolyte

During the history of Li-ion battery, liquid and solid-state electrolytes have been investigated. The older liquid electrolyte technology had safety problems due to the leakage of corrosive or explosive liquids and internal short-circuits. These problems promoted the search for ultimate solid polymer electrolytes that offer an all-solid-state construction, simplicity of manufacture, a wide variety of shapes and sizes, and a higher energy density [42]. Over the past few years, research has focused on two types of polymer electrolyte: solvent-free membranes such as poly(ethylene oxide) with a lithium salt LiX (X = PF_6^- or CF_3SO_3^-) and gel-type membranes such as poly(vinylidene fluoride) matrix [43]. However, the disadvantages of poor ionic conductivity of these electrolytes at room temperature and instability of the lithium metal interface associated with the presence of the liquid component have prevented them from further application.

Various approaches have tried to solve such problems. For solvent-free membranes, approaches include dispersing nanoscale

ceramics and adding large anion lithium salts or anion trapping agents [44]. In the former approach, the improved mechanical, transport, and interfacial properties of PEO–LiX membranes have been confirmed by the addition of nanosized active ceramics [45]. For the latter case, the addition of large anion lithium salts lowers the lattice energy and reduces the electrostatic anion-to-cation attraction, which can then enhance the ion conductivity and increase the working temperature range [46]. While the addition of supermolecular compounds such as calixarene ($C_{72}H_{94}N_6O_{10}$) or calixpyrrole ($C_{72}H_{66}N_6$) serves as anion trapping agents to free the Li-ion transport [47]. For alternative gel-type membranes with wider operating temperature, the membrane formed by trapping a $LiPF_6$ –ethylene carbonate (EC)–propylene carbonate (PC) solution in a poly(vinylidene fluoride) matrix (solid–liquid hybrid, 5.0 V vs. Li^+/Li) exhibits promising mechanical properties (similar to solid polymers), conductivity (comparable to the liquid component) and electrochemical stability (prior to the pure liquids) due to the interactions between the liquid phase and the polymer matrix [48]. Although improved, the challenge still remains. For example, the room-temperature conductivity of solvent-free PEO-based electrolyte is a problem since such a polymer usually operates at a temperature of 70–100 °C. Possibly, further improvement may be achieved by optimizing the battery geometry with the ohmic drops and electrode morphology with the enhancement of Li diffusion. In addition, other avenues are being explored to achieve high-conductivity polymer electrolytes. As a demonstration, crystalline polymer electrolytes with the crystalline complexes $PEO_6:LiXF_6$ ($X = P, As, \text{ and } Sb$) ratio of 6:1 represent a different type of ionic conductivity [49], and the further replacement of the XF_6 ions with other mono or divalent anions enhances the conductivity by two orders of magnitude [50].

To sum up, Li-ion battery technology powers most of today's portable electronic devices (cell phones, digital cameras, laptops, PDA). Such a battery system is expected to take over the electric vehicle (EV) and hybrid electric vehicle (HEV) market. However, the performances of Li-ion batteries are still bottlenecked by intrinsic limitation of current battery materials. In particular, the intrinsic diffusion of Li ions in the solid state (ca. $10^{-13} \text{ cm}^2/\text{s}$ for commercial $LiCoO_2$) inevitably limits its rate of intercalation/de-intercalation. Therefore, new generations of electrode and electrolyte materials for rechargeable Li-ion batteries are under investigation in the area with the combination of faster diffusion kinetics, higher reversible capability and structural stability, lower cost, and more environmental friendliness.

3. Aqueous and non-aqueous atomic/ionic magnesium system, $Mg \leftrightarrow Mg^{2+}$

Mg, with a high theoretical specific capacity (2205 mA h/g) and a more negative electrode potential ($E_{Mg^{2+}/Mg}^0 = -2.73 \text{ V}$ for $Mg \rightarrow Mg^{2+} + 2e$), is undoubtedly a promising anode material for use in battery systems.

3.1. Primary Mg battery

Among aqueous Mg primary batteries, the Mg/air battery exhibits a high theoretical voltage ($E^0 = 3.09 \text{ V}$ for $2Mg + O_2 + 2H_2O \rightarrow 2Mg(OH)_2$), high energy density (3910 W h/kg), and “mechanical recharge” character since the Mg electrode can be easily replaced. Our recent work describes an example of Mg/air battery replacing the commercial Mg power with Mg nano/mesoscale (spheres, plates, rods, sea-urchin-like) structures as the anode [51]. The results show that the Mg/air battery made from Mg sea-urchin-like nanostructures displays better electrochemical properties than that of the batteries with the other Mg nano/mesostructures. This improvement is attributed to the porous

and network structure of the nanostructures, which display lower anodic polarization/corrosion of Mg and faster sedimentation of the anodic product ($Mg(OH)_2$) in the electrolyte.

3.2. Secondary Mg battery

A non-aqueous Mg secondary battery has been mainly pioneered by Aurbach's group [5]. The components of the Mg secondary battery include Mg metal or Mg alloy anode, $Mg_xMo_6S_8$ ($0 < x < 2$) Chevrel phase cathode and electrolyte solutions ($R_2Mg + AlCl_3-nR_n$ in ethereal solvents). With respect to Mg or Mg alloy anode, the morphologies of the deposited Mg have a clear correlation with the cycling efficiency of Mg anode, and a porous deposition is superior to a compact or crystalline deposit [52].

For electrolyte, previous experiments have found that electrolyte solutions for Mg deposition must be polar aprotic such as ethereal solutions of Mg Grignard reagents, amidomagnesium halides, $Mg(BR_2R'_2)_2$ ($R, R' = \text{alkyl or aryl group}$), and $Mg(AX_{4-n}R_nR'_n)_{n'}$ ($A = Al \text{ and } B; X = Cl \text{ and } Br; R, R' = \text{alkyl or aryl group}$) in ethereal or THF solutions [53–56]. This character is due to the fact that Mg anode can be easily passivated in aqueous solutions or protic solvents (alkyl carbonates, esters, and acetonitrile), and the organic/inorganic Mg salts generated on the electrode surface will prevent the migration of Mg^{2+} . The best electrolyte developed so far is the ether/ $(MgR_2)_n(AlCl_2R)_m$ [57]. To further widen the electrochemical window with a higher redox potential and higher capacity than Chevrel phases, a new solution prepared from phenyl-MgCl and $AlCl_3$ has recently been reported, in which all the organic ligands are phenyl groups. The results show a wider electrochemical window (lower by 0.1 V than $MgBu_2(AlCl_2Et)_2$), higher ionic conductivity (increased by a factor of 2–3) and faster kinetics of Mg deposition/dissolution processes [58].

In the area of Mg-ion battery cathode, the kinetics of Mg diffusion in the Chevrel phases is strongly influenced by composition and temperature. For example, at low temperature, some of the Mg^{2+} ions (ca. 20–25%) are trapped in the micrometric size $Mg_xMo_6S_8$ ($0 < x < 2$) and only 75–80% of the theoretical capacity could be reached. Much research has focused on the modification of typical Chevrel phases (namely $M_xMo_6T_8$, $M = \text{metal}$; $T = S \text{ and } Se$), as schematically shown in Fig. 6 [59]. The ‘Chevrel phase’ is a stacking of Mo_6T_8 ($T = S \text{ and } Se$) blocks composed of the octahedral cluster of molybdenum atoms inside the S/Se cube. For $MgMo_6S_8$, the Mg ion is distributed statistically between inner sites (Fig. 6a). For $Mg_2Mo_6S_8$, some Mg ions are located in the inner sites and other Mg ions in the outer sites (Fig. 6b). Replacing small amounts of S by Se can release the trapping Mg^{2+} to improve the kinetics of the Mg^{2+} cations in Chevrel phases. Furthermore, with the benefit of nano-size Chevrel phases as the active material, improved kinetics could be obtained due to the high surface area and short diffusion length. In addition to Chevrel phases, any transition-metal oxide or sulfide with high specific capacity and ionic mobility could theoretically serve as the cathode. Tao et al. have successfully applied titanium disulfide (TiS_2) nanotube as the cathode materials of rechargeable Mg-ion batteries, showing relatively high-capacity and good-reversibility properties [60]. Until now, the efforts are still concentrated on finding suitable electrolyte solutions with a wide electrochemical window, new cathode materials, and a simple synthesis procedure for the components of rechargeable Mg batteries [61].

4. Aqueous molecular/atomic hydrogen and proton system, $H_2(H) \leftrightarrow H^+$

4.1. Profile of $H_2(H)/H^+$ system, hydrogen fuel cells

In the future, the most promising hydrogen/proton systems are the hydrogen fuel cells (HFCs). A HFC is designed as a kind

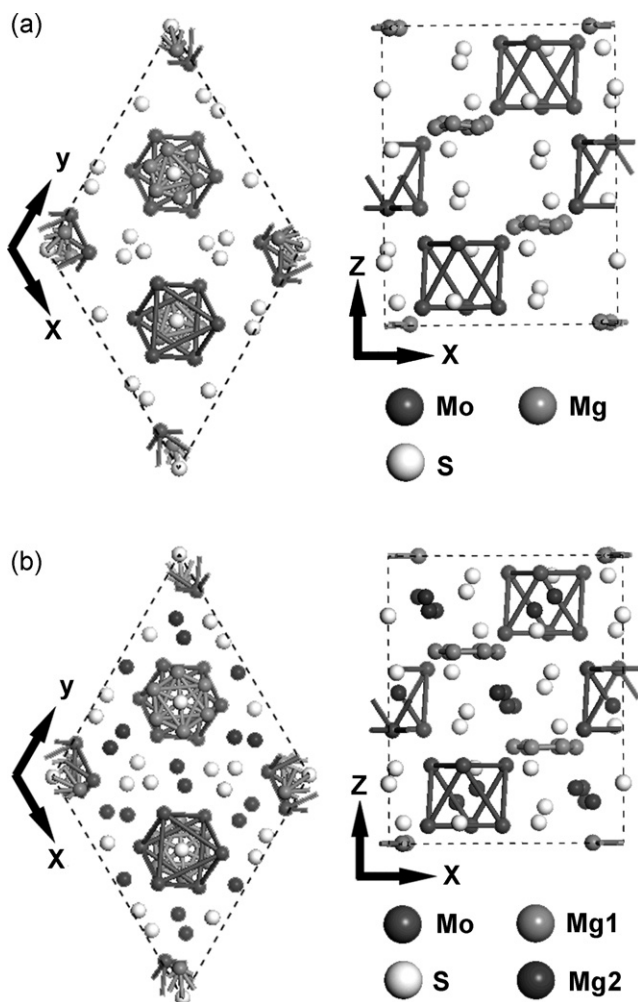


Fig. 6. Crystal structures of Chevrel phases. (a) MgMo_6S_8 : $a=b=9.4592714(6)$ Å and $c=10.5588446(5)$ Å; $\alpha=\beta=90^\circ$, $\gamma=120^\circ$; space group, $R\bar{3}$. (b) $\text{Mg}_2\text{Mo}_6\text{S}_8$: $a=b=9.7630596(10)$ Å and $c=10.3689375(10)$ Å; $\alpha=\beta=90^\circ$, $\gamma=120^\circ$; space group, $R\bar{3}$. Data are taken from Ref. [59].

of device that transforms chemical energy to electrical energy through the electrochemical reaction of hydrogen and oxygen. The advantages of HFC include high energy density, high energy conversion efficiency (without Carnot cycle limitations), modular construction, non-polluting, low maintenance, silence, and safety. The disadvantages of HFC include high cost for catalysts and electrolyte, intolerant of impurities, low power density, and limited life. The basic reaction of a HFC contains an oxidation half-cell reaction ($2\text{H}_2 \rightarrow 4\text{H}^+ + 4\text{e}^-$) and a reduction half-cell reaction ($\text{O}_2 + 4\text{H}^+ + 4\text{e}^- \rightarrow 2\text{H}_2\text{O}$), giving a total reaction of $2\text{H}_2 + \text{O}_2 = 2\text{H}_2\text{O}$ ($E^0 = 1.229\text{ V}$) [62].

Fig. 7 shows a typical kind of hydrogen fuel cell, namely, proton exchange membrane fuel cell (PEMFC), which is composed of bipolar plate as electrode with in-milled gas channel structure and polymer electrolyte membrane (PEM). The workflow of a PEMFC follows. First, a stream of hydrogen is delivered through field flow plates to the anode side and catalytically split into protons and electrons by a platinum catalyst. Then, the protons pass through the PEM to the cathode where the electrons (traveling through the external circuit) and the protons react with oxygen electrochemically to form water, which finally flows out of the PEMFC. The most critical components of the PEMFC include PEM, catalytic electrode, and hydrogen production and storage, which will be overviewed in the following sections.

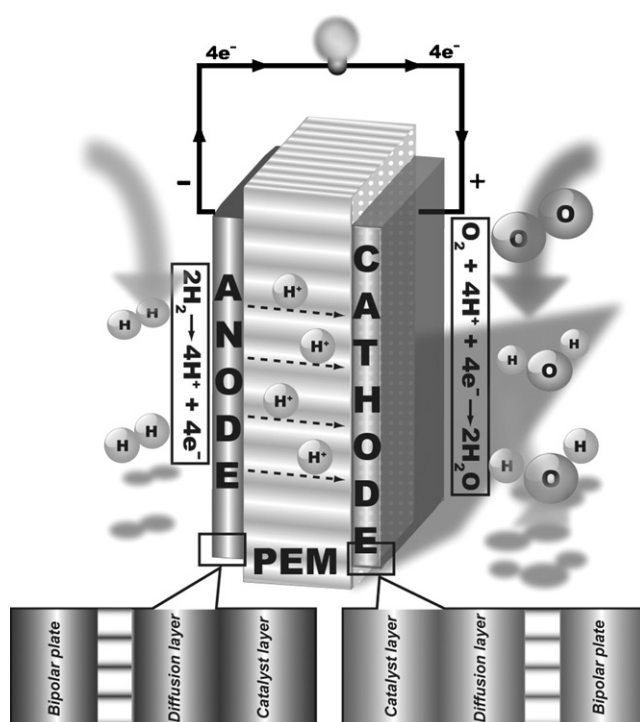


Fig. 7. Profile of a typical hydrogen–oxygen fuel cell.

4.2. Proton exchange membranes

The PEM is a proton conductor and also acts as separator and base of the “active mass” [63]. A high performance PEM should satisfy the following basic requirements: (1) high proton conductivity and low electron conductivity over 100°C ; (2) adequate mechanical strength under both dry and swollen states; (3) high chemical and electrochemical stability under operating conditions; (4) good water management; (5) high durability; (6) low fuel (H_2) and oxidant (O_2) crossover; and (7) low production cost.

The vast majority of the commercially available membranes are based on Nafion, whose chemical structure is shown in Fig. 8. The commonly used Nafion is a sulfonated tetrafluoroethylene copolymer backbone with pendant side chains of perfluorinated vinyl ethers terminated by perfluorosulfonic acid groups [64]. The backbone is hydrophobic and makes the water concentrate in the pores of the Nafion when hydrated. The proton conductivity of Nafion results from the interaction between acid groups in the organic membrane materials and the absorbed water. There is a high ionic conductivity of about 0.08 S/cm obtained for Nafion at 25°C in a 100% humidity environment) [65]. For further optimization, a detailed knowledge of the chemical microstructure and nanoscale morphology of Nafion is required. Mainly due to the limited understanding of the electrochemical reactions during fuel cell operations, the hierarchical structure of the Nafion is still a mystery. Recently, Schmidt-Rohr and Chen have proposed a 3D numerical model solving the transport properties of hydrated Nafion and could allow for the anisotropic optical and mechanical properties [66].

Other similar materials have been developed and commercialized, such as Asahi Glass Company's Flemion, Asahi Chemical Industry's Aciplex and Dow Chemical's membrane [67]. However, most of the membranes are too expensive for large-scale applications and suffer from low conductivity at low water content, low mechanical strength at higher temperature, and moderate glass transition temperatures. To obtain better mechanical strength and dimensional stability, Bahar et al. have developed a composite

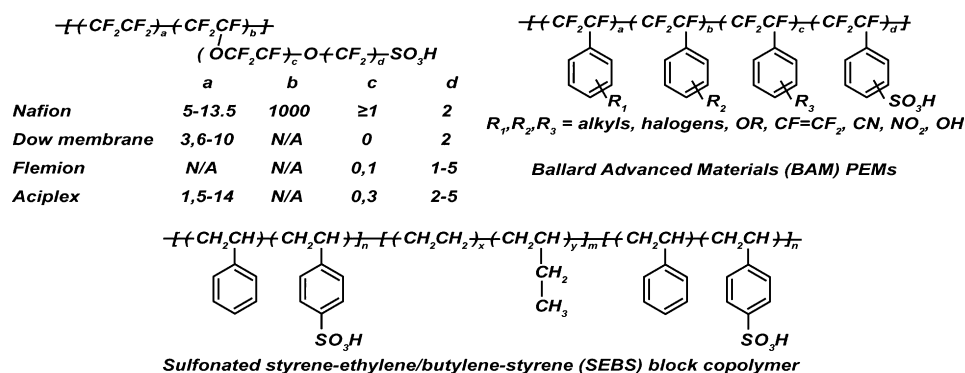


Fig. 8. Selected commercially available proton exchange membranes.

membrane, in which Nafion is filled throughout an inert Teflon-like matrix [68]. The water uptake of this kind of membrane is about 15 water molecules per sulfonic acid group and the proton conductivity lies within the range 10^{-2} to 10^{-1} S/cm. Incorporation with nanostructures could improve the performance of PEMFCs. For example, Pt nanoparticles prevent fuel (H_2) and oxidant (O_2) crossover, and the metal oxide particles such as ZrO_2 , TiO_2 , and SiO_2 improve the water retention properties of Nafion [69–71]. The nanostructures also benefit by reducing the membrane resistance for proton conduction. By blending Nafion with 3 wt% titanium dioxide particles, the conductivity of Nafion membranes can be increased by about 20% [72].

With much less expense, two other membranes have been used in PEMFCs, namely, Ballard Advanced Materials (BAMs) PEMs produced by Ballard Technologies Corporation and Dais Analytic's sulfonated styrene-ethylene-butylene-styrene (SEBS) membrane. Both membranes are based on styrene or styrene-like monomers. Better performance can be achieved with the BAM membranes, compared with Nafion 117 and Dow membranes, at current densities >0.6 A/cm 2 and the lifetime of the assembled Ballard Mk-5 single cell is greater than 15,000 h [73]. Due to the poor oxidative stability, DAIS membranes are mainly used in portable fuel cell power sources of 1 kW [63]. There are also efforts to focus on hydrocarbon polymers membranes. The competitive advantages of hydrocarbon polymers are low cost, high water uptake over a wide temperature range due to the polar groups, improved stability by proper molecular design, and easy recycling [74].

Currently, Nafion still remains the benchmark material against which most results are compared. However, with the deeper understanding of the finer structural detail of the membranes and the more experiment and theoretical data obtained, significant progress can be expected.

4.3. Electrode/catalyst

In the process of fuel cell operation, platinum is the most common catalyst for both oxygen reduction and hydrogen oxidation reactions that take place at the surface of the catalyst layer. The biggest challenge in this area is to reduce the material cost, which is considered to be solved either by increasing the activity of Pt-based catalysts or by developing other non-noble metal catalysts [75]. In the former case, Pt particles supported on activated carbon (or Vulcan XC 72R) are usually used as the catalysts. A high dispersion of Pt can reduce its amount in the catalyst. In particular, there have been many methodologies such as sputtering deposition, polymer mediation, and lithiation/de-lithiation of submicrometer PtO_2 developed to prepare Pt nanoparticles with narrow size distribution (2–4 nm), which can be finely dispersed on the surface of carbon powders [76–78]. Additionally, various novel Pt nanostructures with high specific surface areas have been synthesized.

For example, Liang et al. prepared hollow nanospheres (ca. 20 nm) consisting of Pt nanoparticles with 2 nm, which exhibit enhanced electrocatalytic activity [79]. Tian et al. reported that tetrahexahedral Pt nanocrystals with high-index facets (such as {7 3 0}, {2 1 0}, and {5 2 0}) show high catalytic activity for electro-oxidation due to the large density of atomic steps and dangling bonds [80]. Remarkably, a two-electron reduction of oxygen exists and the H_2O_2 formed could reduce the efficiency of a PEMFC by degrading the catalytic activity of catalysts and/or attacking the catalyst support [81]. Impurities such as CO, H_2S , NH_3 , organic sulfur-carbon and carbon-hydrogen compounds in the H_2 stream, and NO_x or SO_x in the air stream can poison the Pt catalyst [82]. To overcome these drawbacks, Pt-transition-metal alloys and non-noble metal alternatives have been investigated [83,84]. Unfortunately, none of these materials has sufficient stability in the acidic environment of PEMFC or has the competitive catalytic activity to that of Pt electrocatalysts.

4.4. Hydrogen production and storage

For the commercialization of PEMFCs, in addition to the suitable membranes and electrode catalysts, hydrogen production and storage are two other important issues that should be mentioned.

Since hydrogen does not occur in nature as a diatomic molecule (H_2) but exists in the form of chemical compounds (water and hydrocarbons), it is usually produced using diverse domestic resources such as fossil fuel and renewable biomass, wind, or solar sources. Commercially, about 95% of the hydrogen is produced by natural gas reforming, which is not a sustainable option and limited by the supply of hydrocarbon fossil fuel. Alternatively, "solar energy" to "hydrogen energy" represents a clean route and hydrogen can be produced primarily by driving water electrolysis with photoelectrochemical cells or by direct photocatalytic splitting of water [85–88]. For the former, the solar to electric energy conversion with solar cells is an established technology (Fig. 9a). However, most of the current solar cells are not suitable for hydrogen generation due to the unfavorable cost of solar cell materials with Si, CdTe, $CuInSe_2$, or GaAs. Instead, direct photocatalytic splitting of water (Fig. 9b) represents a promising alternative owing to the low price and high stability of the photocatalysts [89–91]. At present, the most intensively investigated photocatalysts are semiconducting metal oxides such as TiO_2 , ZnO, WO_3 , and Fe_2O_3 . Especially, nanostructures of the semiconductors exhibit novel properties that may make solar-hydrogen production commercially viable in the future. For example, since the band gap energy of bulk TiO_2 (3.0–3.2 eV) does not match the value (~ 1.7 eV) for efficiently absorption in the visible region, various kinds of nanostructured TiO_2 (nanofilms, nanowires, nanotubes, or nanocomposites) have been prepared to decrease the band gap for efficient absorption of visible light and increase the photocatalytic reactions [92,93].

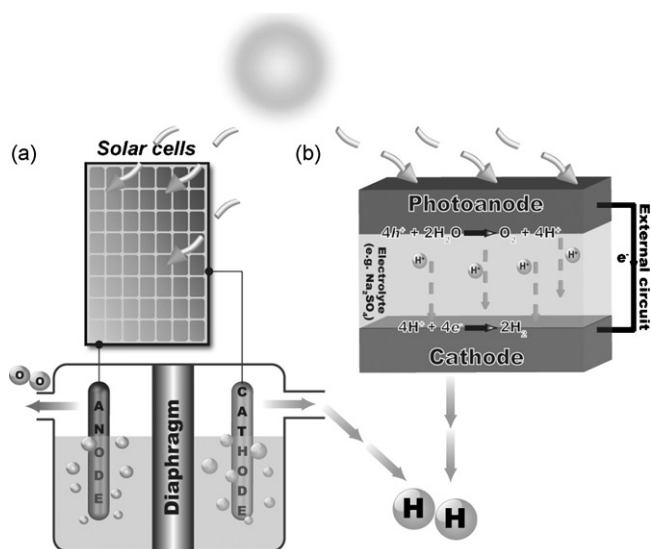


Fig. 9. Two primary ways which currently utilize a solar source to produce H_2 : (a) driving water electrolysis with solar cells and (b) direct photocatalytic splitting of water.

With respect to hydrogen storage, the current challenge is to develop on-board hydrogen storage materials with the combination of high gravimetric/volumetric hydrogen density, adequate kinetics, reversibility, low cost, and low toxicity. To meet these targets, many kinds of solid materials have been investigated [94–99], typically: (1) MgH_2 and Mg-based alloy/complex hydrides; (2) NH_3BH_3 , LiBH_4 , NaBH_4 , LiAlH_4 , NaAlH_4 chemical hydrides; (3) metal nitrides and imides (Li_3N and LiNH_2); (4) advanced carbon nanomaterials, metal–nonmetal inorganic compound (TiS_2 and MoS_2) nanostructures, and metal–organic frameworks (MOFs).

Since none of the present materials could satisfy all the requirements for hydrogen storage application, attention has been mainly concentrated on modifying the materials physically or chemically. Mg/ MgH_2 system is a typical example. In order to increase the desorption rates and lowering the desorption temperature of MgH_2 , different strategies have been tried, mainly involving alloying Mg with other elements and synthesizing Mg/ MgH_2 nanostructures. In the former case, Mg-based transition-metal complex hydrides such as Mg_2NiH_4 , Mg_2CoH_5 , and Mg_2FeH_6 have been widely investigated [100]. These compounds usually follow an 18-electron rule resulting from their ionic character additionally to crystal field effects (Fig. 10) [101–104]. The doping transition metals (Ni, Co and Fe) are coordinated by four to six H atoms to form the anions, namely $[\text{NiH}_4]^{4-}$, $[\text{CoH}_5]^{4-}$ and $[\text{FeH}_6]^{4-}$, which possess mixed ionic–covalent bonds. The absorbed hydrogen atoms mainly intercalate the Mg^{2+} lattice. The structural properties then improve the sorption kinetics drastically, but the thermodynamics are less affected.

As an alternative, nanostructured Mg/ MgH_2 has been tried as a potential medium. By physical vapor deposition, our group has synthesized Mg nanowires with diameters ranging from ~30 to 170 nm, and the kinetics of both the adsorption and desorption processes are obviously enhanced [105]. Aguey-Zinsou et al. reported that, with the help of surfactant, Mg nanoparticles of 5 nm can be obtained and the corresponding colloidal MgH_2 desorb full hydrogen at 85°C [106]. Recently, first principles calculations based on density functional theory have demonstrated that ca. 2 nm Mg/ MgH_2 nanostructures show significant change in thermodynamics [107–110]. Future advances may involve the design and synthesis of Mg-based materials for hydrogen storage at near-room temperature.

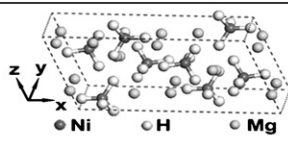
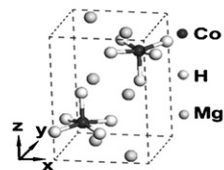
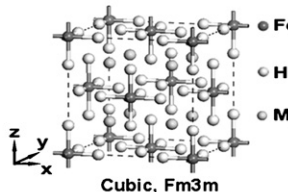
Hydride	Crystal structure	18-Electron structure (Mg: $3s^2$; H: $1s^2$)	H/wt%
Mg_2NiH_4	 Monoclinic, $C2/c$ $a=14.343 \text{ \AA}$, $b=6.4038 \text{ \AA}$, $c=6.4830 \text{ \AA}$, $\beta=113.5^\circ$	Ni: $3d^8 4s^2$ $18=2\times 2+8+2+1\times 4$	3.6
Mg_2CoH_5	 Tetragonal, $P4/nmm$ $a=4.480 \text{ \AA}$, $c=6.619 \text{ \AA}$	Co: $3d^7 4s^2$ $18=2\times 2+7+2+1\times 5$	4.5
Mg_2FeH_6	 Cubic, $Fm\bar{3}m$ $a=6.443 \text{ \AA}$	Fe: $3d^6 4s^2$ $18=2\times 2+6+2+1\times 6$	5.5

Fig. 10. Crystal structure, electronic structure and theoretical hydrogen content of 18-electron structural Mg_2NiH_4 , Mg_2CoH_5 and Mg_2FeH_6 . Data are taken from Refs. [101–104].

5. Conclusions and outlook

In summary, we have briefly reviewed the recent development of functional materials applied in the energy storage and conversion systems with non-aqueous atomic/ionic rechargeable Li-ion battery, primary and secondary Mg battery, and aqueous molecular/atomic hydrogen/proton related fuel cells. For rechargeable Li-ion batteries, effort has focused on utilizing nanostructured anode/cathode materials to improve the battery performance. Nanomaterials show favorable properties such as enhanced kinetics and activity, while nanosize effects also bring low thermodynamic stability, high side-reactions as well as handling problems. For the less developed rechargeable Mg-ion battery, both opportunities and challenges exist. In this new energy conversion system, the search for new electrolyte solutions with a wider electrochemical window for Mg electrodes and for new cathode materials with high capacity and redox potential are especially important. In the area of hydrogen fuel cells, the subjects of PEM, catalytic electrode, and hydrogen production and storage have been addressed for developing less expensive and more efficient proton exchange membranes, electrocatalysts, and hydrogen storage materials/systems.

Acknowledgements

This work was supported by the Programs of National NSFC (50631020, 50771056 and 20873071), 973 (2005CB623607) and Tianjin Basic Research (08JCZDJC21300).

References

- [1] D. Linden, T.B. Reddy, Handbook of Batteries, Third edition, McGraw-Hill, New York, 2002.
- [2] M. Winter, R.J. Brodd, Chem. Rev. 104 (2004) 4245.
- [3] <http://www.en.wikipedia.org/wiki/>.
- [4] F.Y. Cheng, Z.L. Tao, J. Liang, J. Chen, Chem. Mater. 20 (2008) 667.

- [5] D. Aurbach, Z. Lu, A. Schechter, Y. Gofer, H. Gizbar, R. Turgeman, Y. Cohen, M. Moshkovich, E. Levi, *Nature* 407 (2000) 724.
- [6] K.J. Takeuchi, A.C. Marschilok, S.M. Davis, R.A. Leising, *Coord. Chem. Rev.* 219–221 (2001) 283.
- [7] B.C.H. Steele, A. Heinzel, *Nature* 414 (2001) 345.
- [8] M. Tarascon, M. Armand, *Nature* 414 (2001) 359.
- [9] Y. Wang, G.Z. Cao, *Adv. Mater.* 20 (2008) 2251.
- [10] N. Douakha, M. Holzapfel, E. Chappel, G. Chouteau, L. Croguennec, A. Ott, B. Ouladdiaf, *J. Solid State Chem.* 163 (2002) 406.
- [11] Y.I. Yang, B.J. Neudecker, N.J. Dudney, *Electrochem. Solid State Lett.* 4 (2001) A74.
- [12] A.K. Padhi, K.S. Nanjundaswamy, J.B. Goodenough, *J. Electrochem. Soc.* 144 (1997) 1188.
- [13] A.S. Andersson, B. Kalska, L. Haggstrom, J.O. Thomas, *Solid State Ionics* 130 (2000) 41.
- [14] D. Morgan, A. Van der Ven, G. Ceder, *Electrochem. Solid State Lett.* 7 (2004) A30.
- [15] K.S. Park, S.B. Schougaard, J.B. Goodenough, *Adv. Mater.* 19 (2007) 848.
- [16] Y.S. Hu, Y.G. Guo, R. Dominko, M. Gaberscek, J. Jamnik, J. Maier, *Adv. Mater.* 19 (2007) 1963.
- [17] B. Kang, G. Ceder, *Nature* 458 (2009) 190.
- [18] X. Li, W. Li, H. Ma, J. Chen, *J. Electrochem. Soc.* 154 (2007) A39.
- [19] K. Lee, Y. Wang, G.Z. Cao, *J. Phys. Chem. B* 109 (2005) 16700.
- [20] N.S. Ergang, J.C. Lytle, K.T. Lee, S.M. Oh, W.H. Smyrl, A. Stein, *Adv. Mater.* 18 (2006) 1750.
- [21] Y.D. Kondrashev, A.I. Zaslavskii, *Izvestiya Akademii Nauk SSSR, Seriya Fizicheskaya* 15 (1951) 179.
- [22] A.A. Bolzan, C. Fong, B.J. Kennedy, C.J. Howard, *Aust. J. Chem.* 46 (1993) 939.
- [23] C. Fong, B.J. Kennedy, M.M. Elcombe, *Zeitschrift fuer Kristallographie* 209 (1994) 941.
- [24] M. Sugantha, P.A. Ramakrishnan, A.M. Hermann, C.P. Warmingsingh, D.S. Ginley, *Int. J. Hydrogen Energy* 28 (2003) 597.
- [25] F.Y. Cheng, J. Chen, *J. Mater. Res.* 21 (2006) 2744.
- [26] F.Y. Cheng, J.Z. Zhao, W.E. Song, C.S. Li, H. Ma, J. Chen, P.W. Shen, *Inorg. Chem.* 45 (2006) 2038.
- [27] T.W. Kim, D.H. Park, S.T. Lim, S.J. Hwang, B.K. Min, J.H. Choy, *Small* 4 (2008) 507.
- [28] F. Jiao, P.T. Bruce, *Adv. Mater.* 19 (2007) 657.
- [29] Z.H. Liu, X.J. Yang, Y. Makita, K. Ooi, *Chem. Mater.* 14 (2002) 4800.
- [30] B.A. Boukamp, G.C. Lesh, R.A. Huggins, *J. Electrochem. Soc.* 128 (1981) 725.
- [31] A.M. Wilson, J.R. Dahn, *J. Electrochem. Soc.* 142 (1995) 326.
- [32] H. Ma, F.Y. Cheng, J. Chen, J.Z. Zhao, C.S. Li, Z.L. Tao, J. Liang, *Adv. Mater.* 19 (2007) 4067.
- [33] C.K. Chan, H.L. Peng, G. Liu, K. McIlwrath, X.F. Zhang, R.A. Huggins, Y. Cui, *Nat. Nanotechnol.* 1 (2008) 31.
- [34] S.G. Ng, J.Z. Wang, D. Wexler, K. Konstantinov, Z.P. Guo, H.K. Liu, *Angew. Chem. Int. Ed.* 45 (2006) 6896.
- [35] J. Hassoun, S. Panero, P. Simon, P. Louis, P.L. Taberna, B. Scrosati, *Adv. Mater.* 19 (2007) 1632.
- [36] P. Poizat, S. Laruelle, S. Grugeron, L. Dupont, J.M. Tarascon, *Nature* 407 (2000) 496.
- [37] H.S. Zhou, D.L. Li, M. Hibino, I. Honma, *Angew. Chem. Int. Ed.* 44 (2005) 797.
- [38] J. Chen, L.N. Xu, W.Y. Li, X.L. Gou, *Adv. Mater.* 17 (2005) 582.
- [39] L. Taberna, S. Mitra, P. Poizat, P. Simon, J.M. Tarascon, *Nat. Mater.* 5 (2006) 567.
- [40] W. van Schalkwijk, B. Scrosati (Eds.), *Advances in Lithium-Ion Batteries*, Kluwer Academic/Plenum, New York, 2002.
- [41] Y. Oumellal, A. Rougier, G.A. Nazri, J.M. Tarascon, L. Aymard, *Nat. Mater.* 7 (2008) 916.
- [42] W. Linert, A. Camard, M. Armand, C. Michot, *Coord. Chem. Rev.* 226 (2002) 137.
- [43] B. Scrosati, *Chem. Rec.* 1 (2001) 173.
- [44] B. Scrosati, *Chem. Rec.* 5 (2005) 286.
- [45] A.S. Arico, P. Bruce, B. Scrosati, J.M. Tarascon, W. van Schalkwijk, *Nat. Mater.* 4 (2005) 366.
- [46] G.B. Appetecchi, D. Zane, B. Scrosati, *J. Electrochem. Soc.* 151 (2004) A1369.
- [47] W. Wieckzorek, E. Peled, D. Golodnisky, G.B. Appetecchi, B. Scrosati, *J. Electrochem. Soc.* 151 (2004) A1762.
- [48] G.B. Appetecchi, P. Romagnoli, B. Scrosati, *Electrochem. Commun.* 3 (2001) 281.
- [49] Z. Gadjourova, Y.G. Andreev, D.P. Tunstall, P.G. Bruce, *Nature* 412 (2001) 520.
- [50] A.M. Christie, S.J. Lilley, E. Staunton, Y.G. Andreev, P.G. Bruce, *Nature* 433 (2005) 50.
- [51] W.Y. Li, C.S. Li, C.Y. Zhou, H. Ma, J. Chen, *Angew. Chem. Int. Ed.* 45 (2006) 6009.
- [52] D. Aurbach, A. Schechter, M. Moshkovich, *J. Electrochem. Soc.* 148 (2001) A1004.
- [53] Z. Lu, A. Schechter, M. Moshkovich, D. Aurbach, *J. Electroanal. Chem.* 466 (1999) 203.
- [54] C. Liebenow, Z. Yang, P. Lobitz, *Electrochem. Commun.* 2 (2000) 641.
- [55] D. Aurbach, H. Gizbar, A. Schechter, O. Chusid, H.E. Gottlieb, Y. Gofer, I. Goldberg, *J. Electrochem. Soc.* 149 (2002) A115.
- [56] J.F. Garst, M.P. Soriaga, *Coord. Chem. Rev.* 248 (2004) 623.
- [57] D. Aurbach, B. Markovsky, G. Salitra, E. Markevich, Y. Talyossef, M. Koltypin, L. Nazar, B. Ellis, *J. Power Sources* 165 (2007) 491.
- [58] E. Levi, E. Lancry, A. Mitelman, D. Aurbach, G. Ceder, D. Morgan, O. Isnard, *Chem. Mater.* 18 (2006) 5492.
- [59] D. Aurbach, G.S. Suresh, E. Levi, A. Mitelman, O. Mizrahi, O. Chusid, M. Brunelli, *Adv. Mater.* 19 (2007) 4260.
- [60] Z.L. Tao, L.N. Xu, X.L. Gou, J. Chen, H.T. Yuan, *Chem. Commun.* (2004) 2080.
- [61] D. Aurbach, I. Weissman, Y. Gofer, E. Levi, *Chem. Rec.* 3 (2003) 61.
- [62] V. Mehta, J.S. Cooper, *J. Power Sources* 114 (2003) 32.
- [63] M.A. Hickner, H. Ghassemi, Y.S. Kim, B.R. Einsla, J.E. McGrath, *Chem. Rev.* 104 (2004) 4587.
- [64] K.A. Mauritz, R.B. Moore, *Chem. Rev.* 104 (2004) 4535.
- [65] S.B. Brijmohan, M.T. Shaw, *Polymer* 47 (2006) 2856.
- [66] K. Schmidt-Rohr, Q. Chen, *Nat. Mater.* 7 (2008) 75.
- [67] F. Barbir, S. Yazici, *Int. J. Energy Res.* 32 (2008) 369.
- [68] B. Bahar, C. Cavalca, S. Cleghorn, J. Kolde, D. Lane, M. Murthy, G. Rusch, J. New Mater. *Electrochem. Syst.* 2 (1999) 179.
- [69] N.H. Jalani, R. Datta, *J. Membr. Sci.* 264 (2005) 167.
- [70] N.H. Jalani, K. Dunn, R. Datta, *Electrochim. Acta* 51 (2005) 553.
- [71] P. Choi, N.H. Jalani, T.M. Thampian, R. Datta, *J. Polym. Sci. Part B: Polym. Phys.* 44 (2006) 2183.
- [72] M.B. Satterfield, P.W. Majsztrik, H. Ota, J.B. Benziger, A.B. Bocarsly, *J. Polym. Sci. Part B: Polym. Phys.* 44 (2006) 2327.
- [73] R. Devanathan, *Energy Environ. Sci.* 1 (2008) 101.
- [74] M. Rikukawa, K. Sanui, *Prog. Polym. Sci.* 25 (2000) 1463.
- [75] C.R.K. Rao, D.C. Trivedi, *Coord. Chem. Rev.* 249 (2005) 613.
- [76] M. Chen, Y.C. Xing, *Langmuir* 21 (2005) 9334.
- [77] R. Zeis, A. Mathur, G. Fritz, J. Lee, J. Erlebacher, *J. Power Sources* 165 (2007) 65.
- [78] Y.S. Hu, Y.G. Guo, W. Sigle, S. Hore, P. Balaya, J. Maier, *Nat. Mater.* 5 (2006) 713.
- [79] H.P. Liang, H.M. Zhang, J.S. Hu, Y.G. Guo, L.J. Wan, C.L. Bai, *Angew. Chem. Int. Ed.* 43 (2004) 1540.
- [80] N. Tian, Z.Y. Zhou, S.G. Sun, Y. Ding, Z.L. Wang, *Science* 316 (2007) 732.
- [81] *Handbook of Fuel Cells—Fundamentals Technology and Applications*, vol.2, 2003 (Chapter 30).
- [82] X. Cheng, Z. Shi, N. Glass, L. Zhang, J.J. Zhang, D.T. Song, Z.S. Liu, H.J. Wang, J. Shen, *J. Power Sources* 165 (2007) 739.
- [83] L. Zhang, J.J. Zhang, D.P. Wilkinson, H.J. Wang, *J. Power Sources* 156 (2006) 171.
- [84] J. Zhu, F.Y. Cheng, Z.L. Tao, J. Chen, *J. Phys. Chem. C* 112 (2008) 6337.
- [85] N. Papageorgiou, *Coord. Chem. Rev.* 248 (2004) 1421.
- [86] V. Artero, M. Fontecave, *Coord. Chem. Rev.* 249 (2005) 1518.
- [87] J.F. Capon, F. Gloaguen, P. Schollhammer, J. Talarmin, *Coord. Chem. Rev.* 249 (2005) 1664.
- [88] K. Sakai, H. Ozawa, *Coord. Chem. Rev.* 251 (2007) 2753.
- [89] A. Fujishima, K. Honda, *Nature* 238 (1972) 37.
- [90] J.H. Park, S. Kim, A.J. Bard, *Nano Lett.* 6 (2006) 24.
- [91] U. Sahaym, M.G. Norton, J. Mater. Sci. 43 (2008) 5395.
- [92] J. Nowotny, T. Bak, M.K. Nowotny, L.R. Sheppard, *Int. J. Hydrogen Energy* 32 (2007) 2609.
- [93] J. Zhang, Q. Xu, Z.C. Feng, M.J. Li, C. Li, *Angew. Chem. Int. Ed.* 47 (2008) 1766.
- [94] W. Grochala, P.P. Edwards, *Chem. Rev.* 104 (2004) 1283.
- [95] A.M. Seayad, D.M. Antonelli, *Adv. Mater.* 16 (2004) 765.
- [96] A.G. Wong-Foy, A.J. Matzger, O.M. Yaghi, *J. Am. Chem. Soc.* 128 (2006) 3494.
- [97] H.W. Langmi, C.S. McGrady, *Coord. Chem. Rev.* 251 (2007) 925.
- [98] S.I. Orimo, Y. Nakamori, J.R. Eliseo, A. Zuttel, C.M. Jensen, *Chem. Rev.* 107 (2007) 4111.
- [99] P. Chen, M. Zhu, *Materialstoday* 11 (2008) 36.
- [100] K. Yvon, *Encyclopedia of Materials: Science and Technology*, Elsevier Limited, Oxford, UK, 2004.
- [101] J.J. Didisheim, P. Zolliker, K. Yvon, P. Fischer, J. Schefer, M. Gubelmann, A.F. Williams, *Inorg. Chem.* 23 (1984) 1953.
- [102] P. Zolliker, K. Yvon, P. Fischer, J. Schefer, *Inorg. Chem.* 24 (1985) 4177.
- [103] J. Zhang, D.W. Zhou, L.P. He, P. Peng, J.S. Liu, *J. Phys. Chem. Solids* 70 (2009) 32.
- [104] P.V. Jasen, E.A. Gonzalez, G. Brizuela, O.A. Nagel, G.A. Gonzalez, A. Juan, *Int. J. Hydrogen Energy* 32 (2007) 4943.
- [105] W.Y. Li, C.S. Li, H. Ma, J. Chen, *J. Am. Chem. Soc.* 129 (2007) 6710.
- [106] K.F. Aguey-Zinsou, J.R. Ares-Fernández, *Chem. Mater.* 20 (2008) 376.
- [107] S. Cheung, W.Q. Deng, A.C.T. van Duin, W.A. Goddard, *J. Phys. Chem. A* 109 (2005) 851.
- [108] R.W.P. Wagemans, J.H. Lenthe, P.E. de Jongh, A.J. van Dillen, K.P. de Jong, *J. Am. Chem. Soc.* 127 (2005) 16675.
- [109] P. Larsson, C.M. Araujo, J.A. Larsson, P. Jena, R. Ahuja, *Proc. Natl. Acad. Sci. U.S.A.* 15 (2008) 8227.
- [110] L. Li, B. Peng, W. Ji, J. Chen, *J. Phys. Chem. C* 113 (2009) 3007.